

1           **The changing character of twenty-first century precipitation over the**  
2           **western United States in the variable-resolution CESM**

3           Xingying Huang, \* Paul A. Ullrich

4           *Department of Land, Air and Water Resources, University of California, Davis*

5           \*Corresponding author address: Xingying Huang, Department of Land, Air and Water Resources,  
6           University of California Davis, Davis, CA 95616.  
7           E-mail: xyhuang@ucdavis.edu

## ABSTRACT

8 (To be added once the main content settled down)

9     **1. Introduction**

10    Understanding the character of precipitation within a changing climate is a major focus of cli-  
11    mate science, in large part because of the pronounced impacts of water availability on socioe-  
12    conomic and natural systems (Hegerl et al. 2004; Kharin et al. 2007; Scoccimarro et al. 2013).  
13    Among these studies, there has been particular interest in precipitation extremes, which are man-  
14    ifested as drought and heavy precipitation events (Seneviratne et al. 2012). Studies examining  
15    the character of precipitation in a warming world, which utilize models of varying complexity  
16    from simple thermodynamic models through complex coupled climate simulations, suggest that  
17    although atmospheric water vapor is increasing, the associated impacts of increased atmospheric  
18    water vapor on precipitation are far more complicated. Extreme precipitation events are even more  
19    nuanced: Some studies suggest that the intensity of extreme precipitation is projected to increase  
20    under global warming in many parts of the world, even in regions where mean precipitation de-  
21    creases (Tebaldi et al. 2006; Kharin et al. 2007).

22    Although future climate predictions are host to large uncertainties, climate models are nonethe-  
23    less one of the most versatile tools for studying climate variability and extremes events in the  
24    future (Easterling et al. 2000). Global climate models (GCMs) have often been used to investigate  
25    changes in the mean, variability and extremes of climate, as forced with predicted greenhouse  
26    gas (GHGs) concentrations and aerosol emissions. Precipitation extremes, as measured by vari-  
27    ous metrics, are predicted to change by future warming based on the results of these simulations  
28    (Meehl et al. 2006). Several past studies have investigated global impacts (Seneviratne et al. 2012),  
29    but impacts at local and regional scales are more difficult to come by. Although increased GHG  
30    concentrations have contributed to observed intensification of heavy precipitation events over the  
31    tropical ocean (Allan and Soden 2008) and the majority of Northern Hemisphere overland areas

<sup>32</sup> Min et al. (2011), these impacts are much more poorly understood at regional scales due to atmospheric circulation patterns of variability (Trenberth 2011), which are more difficult to assess at  
<sup>33</sup> the coarse model resolutions used in previous studies.

<sup>34</sup> Insufficient regional-scale climate information has been a major outstanding problem in climate  
<sup>35</sup> science, as stakeholders and water managers typically require fine-scale information on climate  
<sup>36</sup> impacts in order to effectively develop adaptation and mitigation strategies. In order to reach the  
<sup>37</sup> scales needed for effective local planning, dynamical downscaling with regional climate models  
<sup>38</sup> (RCMs) has been typically used to ascertain the frequency, intensity, and duration of extreme  
<sup>39</sup> events. By only simulating a limited regional domain, RCMs better capture fine-scale dynamical  
<sup>40</sup> features under high horizontal resolution (Bell et al. 2004; Frei et al. 2006; Rauscher et al.  
<sup>41</sup> 2010; Wehner 2013). Higher resolution can also enable more accurate simulations of precipitation  
<sup>42</sup> extremes, which can be driven by land use, land/water contrast, snow cover, cloudiness and circula-  
<sup>43</sup> tion patterns associated with topography (Leung et al. 2003a; Diffenbaugh et al. 2005; Salathé Jr  
<sup>44</sup> et al. 2008; Wehner et al. 2010). Diffenbaugh et al. (2005) studied both heat events and wet events  
<sup>45</sup> over the contiguous United States based on RCMs simulation at 25 km horizontal resolution, and  
<sup>46</sup> demonstrated that fine-scale processes are critical for accurate assessment of local- and regional-  
<sup>47</sup> scale climate change vulnerability. Leung et al. (2003b) showed that the higher-resolution nests  
<sup>48</sup> utilized by RCMs yield more realistic precipitation patterns and produce more frequent heavy  
<sup>49</sup> precipitation over the western U.S. (WUS), which is in turn more consistent with observations.

<sup>50</sup> Despite their success, RCMs also have known issues associated with inconsistency between the  
<sup>51</sup> lateral forcing data and the driven RCM, and the menu of physical parameterizations typically  
<sup>52</sup> available to RCMs expose the potential for over-tuning the model for a particular geographic  
<sup>53</sup> region (McDonald 2003; Laprise et al. 2008; Mesinger and Veljovic 2013). Consequently, there  
<sup>54</sup> has been growing interest in variable-resolution enabled GCMs (VRGCMs) to improve regional

climate simulations. Unlike RCMs, which require GCM data to drive the simulation at lateral boundaries, VRGCMs use a unified model with coarse global resolution and enhanced resolution over a specific study region (Staniforth and Mitchell 1978; Fox-Rabinovitz et al. 1997). VRGCMs have demonstrated comparable utility for regional climate studies at a reduced computational cost, particular when compared to uniform-resolution GCMs (Fox-Rabinovitz et al. 2006; Rauscher et al. 2013).

In this paper, we utilize the recently developed variable-resolution option in the Community Earth System Model (VR-CESM). VR-CESM is based on the CESM (and its predecessor, the Community Climate System Model (CCSM)), a family of models that have been used for decades to study the global climate (Neale et al. 2010a; Hurrell et al. 2013), and demonstrated competitive ability when contrasted with other climate models. The overall performance of VR-CESM for modeling regional climate in the California and Nevada is detailed in Huang et al. (2016), who argued VR-CESM has competitive biases in comparison to the Weather Research and Forecasting (WRF) model (a traditional RCM), when evaluating both against high-quality observations and reanalysis. VR-CESM has also been employed for other studies and demonstrated that it is competitive at capturing fine-scale atmospheric processes with the uniform-resolution CESM and other RCMs, without apparent artifacts within the coarse-fine transition region (Zarzycki et al. 2014, 2015; Rhoades et al. 2015).

This study focuses changes in the character of precipitation over the 21st Century within the WUS, as predicted from long-term ensemble runs conducted with VR-CESM with a local grid resolution of  $\sim 0.25^\circ$ . The WUS is known to be particularly vulnerable to hydrological extreme events, particularly floods and droughts (Leung et al. 2003b; Caldwell 2010), and features a variety of local features and microclimates associated with its rough and varied topography. Simulations of the future climate are performed in accordance with the representative concentration pathway

80 (RCP) 8.5 scenario, which describes a “business-as-usual” projection for GHGs among other RCPs  
81 (Riahi et al. 2011). RCP 8.5 is a baseline scenario with updated base year calibration (to 2005)  
82 and no explicit climate policy (Riahi et al. 2011) and end-of-century projections with the substan-  
83 tially weaker RCP2.6 scenario are found to be qualitatively similar to mid-century RCP8.5 results.  
84 Simulations are further conducted in accordance with the Atmospheric Model Intercomparison  
85 Project (AMIP) protocol (Gates 1992), a widely-used approach for climate model diagnosis, val-  
86 idation and intercomparison that imposes global sea surface temperatures (SSTs) and sea ice. By  
87 constraining atmospheric boundary conditions at the sea surface, we avoid model biases that are  
88 known to exist in the fully coupled configuration (Grodsy et al. 2012; Small et al. 2014) and  
89 accept potential uncertainties associated with our choice of SSTs.

90 Changes in the character of precipitation, in terms of frequency and intensity, have been assessed  
91 in our study from recent history through the end of 21st century. A comprehensive set of metrics  
92 for precipitation extremes have been evaluated from ensemble simulations over the **26-year** peri-  
93 ods corresponding to historical (1980-2005), mid-century (2025-2050) and end-of-century (2075-  
94 2100). Using this information, it is our goal to improve our understanding of precipitation at  
95 relatively fine spatial scales. We hypothesize that spatial inhomogeneity in local geography and  
96 temperature will also result in similarly inhomogeneous impacts on the precipitation field. We fur-  
97 ther expect that teleconnections (specifically the El Niño-Southern Oscillation (ENSO)) will have  
98 a pronounced impact on precipitation features over particular area under the changes of mean SST  
99 and its variations. Since only one SST dataset was used for this study, we note that our projections  
100 are conditioned on a particular future character of ENSO. This is a potentially large source of  
101 uncertainty, as at present there is no clear consensus on how ENSO may behave under a warming  
102 climate (Fedorov and Philander 2000; Guilyardi et al. 2009), and strengthening or weakening of  
103 this pattern will have clear consequences for our results.

104 This work builds on a number of previous studies that have explored the projected future change  
105 in WUS precipitation. For example, Kim (2005) applied downscaled climate change signals to se-  
106 lected indicators, and concluded that global warming induced by increased CO<sub>2</sub> is likely to drive  
107 increases in extreme hydrologic events in the WUS. Duffy et al. (2006) found that mean precip-  
108 itation predicted by the RCMs are not statistically significant compared to interannual variability  
109 in many regions over WUS, though there is little consistency among the different RCMs as to  
110 responses in precipitation to increased GHGs. Gao et al. (2015) pointed out a potentially large  
111 increase in atmospheric river events by the end of the 21st century under the RCP8.5 scenario.

112 This paper is structured as follows. Section 2 describes the model setup. Section 3 describes  
113 the methodology and reference datasets employed. An assessment of the ability of the model to  
114 capture the climatology of the WUS is given in section 4. Results from the future mean climatol-  
115 ogy trend and projected changes to precipitation indices is in section 6. Section 7 summarizes the  
116 main points of the study along with further discussions.

## 117 2. Model Setup

118 CESM is a state-of-the-art Earth modeling framework, consisting of coupled atmosphere, ocean,  
119 land and sea ice models (Neale et al. 2010b; Hurrell et al. 2013). In this study, Community At-  
120 mosphere Model version 5 (CAM5) (Neale et al. 2010b) and the Community Land Model version  
121 4.0 (Oleson et al. 2010) are used. Within CAM5, we use the Spectral Element (SE) dynamical  
122 core, which incorporates the variable-resolution option (Zarzycki et al. 2014) and includes de-  
123 sirable conservation and parallel scalability properties (Dennis et al. 2011; Taylor 2011). CLM  
124 is employed in the *unigrid* configuration, which allows the land model to be co-located with the  
125 atmospheric grid and so eliminates the need for interpolation. SSTs and sea ice, which are used  
126 to compute ocean-atmosphere fluxes, are prescribed in accordance with the AMIP protocol (Gates

<sup>127</sup> 1992). The variable-resolution mesh used for this study is depicted in Figure 1, in accord with our  
<sup>128</sup> past studies (Rhoades et al. 2015; Huang et al. 2016; Huang and Ullrich 2016).

<sup>129</sup> Simulations have been performed for the historical period (1979-2005, hereafter referred to as  
<sup>130</sup> hist) and for two future periods: 2024-2050 (hereafter referred to as mid) and 2074-2100 (hereafter  
<sup>131</sup> referred to as end). For purposes of analysis, the first year of each time period was discarded as a  
<sup>132</sup> spin-up period to allow adequate time for the initialized land and atmosphere to equilibrate. The  
<sup>133</sup> 26-year duration was chosen to provide an adequate sampling of annual variability for each time  
<sup>134</sup> phase. For future projections, GHG concentrations are set based on RCP8.5. Historical SSTs and  
<sup>135</sup> sea ice are prescribed at  $1^{\circ}$  resolution, as described by Hurrell et al. (2008). SSTs and sea ice  
<sup>136</sup> for each future period are developed from fully-coupled RCP 8.5 climate simulations with bias  
<sup>137</sup> correction applied (Cecile Hannay, personal communication). Using prescribed SSTs in place of  
<sup>138</sup> a coupled ocean model considerably reduces the computation cost and so allows the atmospheric  
<sup>139</sup> model to be run at a higher overall resolution. Annually-updated land surface datasets, which  
<sup>140</sup> prescribe land-use characteristics, are interpolated from  $0.5^{\circ}$  to the land model grid.

<sup>141</sup> Ensemble runs are needed to ensure that the sample adequately accounts for climate variability,  
<sup>142</sup> especially for statistics associated with climatological extremes. However, the exact number of  
<sup>143</sup> ensemble members required is heavily dependent on the variability of the particular metric being  
<sup>144</sup> examined, and so no standard ensemble criteria exists (Deser et al. 2012b). Deser et al. (2012b)  
<sup>145</sup> suggest that around 3 ensemble runs are required to detect a significant epoch difference for JJA  
<sup>146</sup> (June-July-August) surface temperatures, whereas 10 to 30 ensemble members are needed for that  
<sup>147</sup> for DJF (Dec.-Jan.-Feb.) precipitation. In our study, the use of prescribed SSTs does reduce the  
<sup>148</sup> intrinsic variability of the climate system (see supplement), and so we found reasonably converged  
<sup>149</sup> results with two ensemble members for the historical period and four ensemble members for each  
<sup>150</sup> future period.

151    **3. Methodology**

152    *a. Precipitation indices*

153    In order to fully account for the precipitation distributions, daily output over all the years are  
154    utilized in data analysis. We have employed standard indices to characterize precipitation (Tebaldi  
155    et al. 2006; Zhang et al. 2011; Sillmann et al. 2013). Several indices have been examined, including  
156    those defined by the Expert Team on Climate Change Detection and Indices (ETCCDI) (Karl  
157    et al. 1999) that have been primarily adopted in previous studies (Dulière et al. 2011; Sillmann  
158    et al. 2013; Diffenbaugh et al. 2005; Singh et al. 2013) and others such as return levels, dry spell  
159    and wet spell defined by either percentiles or by selected thresholds. As a result, loosely based  
160    on the former studies, the indices we have chosen for this study attempt to provide a relatively  
161    comprehensive characterization of precipitation, along with being easy to interpret and relevant to  
162    stakeholders. The indices employed are summarized in Table 1.

163    *b. Impacts of ENSO*

164    The impact of ENSO on precipitation is emphasized in our study due to its influence on pre-  
165    cipitation over a majority of our study area, particularly in the southwest U.S. (Cayan et al. 1999;  
166    Zhang et al. 2010; Deser et al. 2012a; Yoon et al. 2015). The phase of ENSO (*i.e.* El Niño and La  
167    Niña) is identified each year using the Oceanic Niño Index (ONI), defined as the 3-month running  
168    means of SST anomalies in the Niño 3.4 region (covering 5N-5S, 120-170W based on NOAA  
169    (2013)). An El Niño or La Niña episode is said to occur when the ONI exceeds +0.5 or -0.5  
170    for at least five consecutive months for a water year (*i.e.* from July to June) (NOAA 2013) (see  
171    the supplement). In order to remove the trend in the SST field associated with climate change,  
172    the anomaly is computed against the detrended mean SSTs from the periods 1971-2000, 2020-

<sup>173</sup> 2050 and 2070-2100 for hist, mid and end respectively, using the aforementioned observed and  
<sup>174</sup> predicted SST datasets. As argued by Kao and Yu (2009), an extended Niño 3.4 region may be  
<sup>175</sup> necessary to determine the phase of ENSO – to determine if this was the case, SST anomalies  
<sup>176</sup> were integrated over the region 105-170W, but it was observed that this had no significant impact  
<sup>177</sup> on ONI statistics.

<sup>178</sup> Student's t-test has been used to test whether or not two datasets at each grid point are statis-  
<sup>179</sup> tically equivalent, if the sample population can be adequately described by a normal distribution.  
<sup>180</sup> The normality of a dataset is assessed under the Anderson-Darling test. When the sample popu-  
<sup>181</sup> lations do not approximately follow a normal distribution, Mann-Whitney-Wilcoxon (MWW) test  
<sup>182</sup> is employed in lieu of the t-test. All these tests are evaluated at the 0.05 ( $\alpha$ ) significance level.

<sup>183</sup> (add description of the supplement like what are included; see the `sst_enso.pdf`, mask the land  
<sup>184</sup> (over land, it should be the surface temperature.))

<sup>185</sup> *c. Reference datasets*

<sup>186</sup> Gridded observational datasets and reanalysis of the highest available quality with comparable  
<sup>187</sup> horizontal resolutions to our VR-CESM simulations are used for assessing the simulation qual-  
<sup>188</sup> ity. The use of multiple reference datasets is necessary due to the underlying uncertainty in the  
<sup>189</sup> reference data. Descriptions of the datasets employed are as follows.

<sup>190</sup> **UW Precipitation Dataset:** The UW daily gridded meteorological data is obtained from the  
<sup>191</sup> Surface Water Modeling group at the University of Washington (Maurer et al. 2002; Hamlet  
<sup>192</sup> and Lettenmaier 2005). UW incorporates topographic corrections for the precipitation. The  
<sup>193</sup> dataset is provided at 0.125° horizontal resolution covering the period 1949 to 2010.

194       **NCEP CPC:** This dataset provides gauge-based analysis of daily precipitation from the Na-  
195       tional Oceanic and Atmospheric Administration (NOAA) Climate Prediction Center (CPC).  
196       It is a suite of unified precipitation products obtained by combining all information avail-  
197       able at CPC via the optimal interpolation objective analysis technique. The gauge analysis  
198       covers the Conterminous United States with a fine-resolution at  $0.25^{\circ}$  from 1948-01-01 to  
199       2006-12-31.

200       **North American Regional Reanalysis (NARR):** The is the NCEP (National Centers for En-  
201       vironmental Prediction) high-resolution reanalysis product that provides dynamically down-  
202       scaled data over North America at  $\sim 32$  km resolution and 3-hourly intervals from 1979  
203       through present (Mesinger et al. 2006).

## 204       4. Model Assessment

205       Before proceeding, we first investigate how well the model is able to represent the character  
206       of precipitation over the WUS. Figures 2 and Figure 3 depict the spatial character of the indices  
207       defined in Table 1. Considering the uncertainty within the reference datasets, the mean of the ref-  
208       erences are used to get the difference from the model output. T-test is applied here with UW, CPC  
209       and NARR as the three statistical samples and the historical runs as two samples averaged over  
210       the whole period, determining at each spatial point whether VR-CESM is statistically equivalent  
211       to the references as stippled in 2 and 3.

212       Compared with observations, VR-CESM well represents the spatial pattern of precipitation, with  
213       majority of the precipitation distributed along the northwest coastal area and the mountainous re-  
214       gions of the Cascades and the Sierra Nevada. Compared to the mean of the references, VR-CESM  
215       does overestimate the Pr significantly over most of the relatively dry region for about 0.2 mm to  
216       1.5 mm, especially over the eastern side of the Cascades and both sides of the Sierra Nevada (with

217 relatively difference reaching 50%-150%). This is further reflected in the overestimation of the  
218 non-extreme Pr events frequency (with  $\text{Pr} < 10 \text{mm/day}$ ) since most precipitation over dry area  
219 is associated with low rainy rate days. However, for the western flank of the Sierra Nevada, the  
220 overestimation of the mean Pr is mainly due to the intensified rain rate, which may related with  
221 the strengthened treatment of orographic effects with excessively strong upward winds. Nonethe-  
222 less, the model captures the precipitation features including frequency and intensity satisfactorily  
223 over the main wet region, where most precipitation is resulted from extreme Pr events (when  
224  $\text{Pr} > 10 \text{mm/day}$ ), without significant difference.

225 The corresponding contribution fraction to total precipitation amount of each range defined in  
226 our metrics is also well represented in the model without significant difference, except the western  
227 side of the the Sierra Nevada and eastern flank of the Cascades in the Washington. This suggests  
228 that despite the aforementioned biases, VR-CESM can still capture the overall shape of the precip-  
229 itation distributions. Biases in simulating extreme precipitation over the topographically complex  
230 regions including the Cascades and Sierra Nevada ranges have also been found by in the high-  
231 resolution simulation by RCMs Walker and Diffenbaugh (2009); Singh et al. (2013), and have  
232 been primarily attributed to excessively strong winds. Biases with the excessively dry eastern  
233 flanks of these mountains may also be associated with the diagnostic treatment of precipitation  
234 species in CESM.

235 As further supported in Huang et al. (2016) by evaluating VR-CESM also at  $0.25^\circ$  for long-term  
236 regional climate modeling over California, it is found that VR-CESM can adequately represented  
237 regional climatological patterns with high spatial correlations. VR-CESM shows comparable per-  
238 formance as WRF at 27 km, but still overestimated overall winter precipitation (about 25%-35%)  
239 compared to reference datasets, with statistically significant difference over the western edge of  
240 the Sierra Nevada, which can be alleviated by increasing the spatial resolution due to improved

241 treatment of orographic effects [Paul: Alan's done some work with refining this region down to  
242 4km and observed the biases were persistent] . The spatial pattern of variability agrees well be-  
243 tween VR-CESM and references and when assessing the frequency of strong precipitation events,  
244 VR-CESM matched closely to the UW dataset everywhere except the Central Valley.

245 CESM at 1 degree resolution was also assessed in order to better understand the impacts of reso-  
246 lution. We find that precipitation patterns over complex topography are poorly represented without  
247 capturing the spatial patterns induced by orographic effects over the Cascades and Sierra Nevada  
248 by uniform CESM at 1 degree, with total precipitation greatly underestimated, when compared to  
249 VR-CESM, gridded data and reanalysis (see the supplement). Basically, the precipitation has been  
250 smooth out at the coastal area and the mountainous regions over northwest U.S when simulated  
251 with CESM at coarse resolution. This result clearly captures the benefits of high resolution (par-  
252 ticularly the representation of topography) in simulating precipitation features. Results are also  
253 provided for the output from a globally uniform CESM run at  $0.25^\circ$  spatial resolution with the  
254 finite volume (FV) dynamical core (Wehner et al. 2014), exhibiting comparable performance to  
255 VR-CESM (see the supplement).

256 We have also assessed the ENSO effect modeled by VR-CESM identified by the difference of  
257 precipitation behaviors between the warm phase (i.e. El Niño) and cool phase (i.e. La Niña)  
258 of ENSO, compared to references (see the supplement). The impact of ENSO for observational  
259 precipitation has a weaker signal compared to the VR-CESM, which might suggest that the model  
260 has an overestimation of ENSO's impact on precipitation, especially over the northwest U.S. The  
261 improvement of ENSO in the model is directly proportional to the representation of ENSO forced  
262 precipitation anomalies (AchutaRao and Sperber 2006). (Is it ok to put it here?)

263 (For the t-test among different time periods, I use the yearly values of each run.)

264 **5. Drivers of climatological precipitation**

265 [Paul: This section needs to be corrected for grammar]

266 Precipitation has been observed and modeled to being changed regionally and globally under  
267 climate warming as discussion in the introduction part as discussed in the introduction. According  
268 to Min et al. (2011), the observed intensification of heavy precipitation events over the the latter  
269 half of the twentieth century are attributed to the human-induced increases in GHGs over majority  
270 of Northern Hemisphere land areas, though no significant changes in total precipitations could be  
271 observed globally (Trenberth 2011). With the combined effects of CO<sub>2</sub> increase and SST increase  
272 in future, the precipitations are assumed to be changed driven by both the radiative changes in  
273 the lower troposphere and increased water vapor evaporation over the ocean (Allen and Ingram  
274 2002; Sugi and Yoshimura 2004). Precipitation extremes are projected to be intensified continually  
275 through the end of 21st century in the both dry and wet regions globally with heterogeneous spatial  
276 patterns (Donat et al. 2016).

277 As described by the Clausius-Clapeyron (C-C) equation, the water vapor content is supposed to  
278 increase by ~7% for each 1°C increase in temperature (Allan and Soden 2008). Evaporation over  
279 the ocean will increase, but may be limited over land due to limitations on soil moisture (Cayan  
280 et al. 2010). However, when the air holds more water vapor, the chances of heavy rain events tend  
281 to increase even when even where total precipitation is decreasing (Trenberth 2011), given that  
282 global total precipitation are expected to increase at a lower rate than precipitation extremes (Al-  
283 lan and Soden 2008). According to previous studies (e.g. (Allan and Soden 2008; O'Gorman and  
284 Schneider 2009; Min et al. 2011)), changes in more extreme precipitation follow the C-C relation-  
285 ship more closely than total precipitation precipitation amount (Trenberth et al. 2003). However,  
286 these changes are still remain uncertain with the rate of increase of precipitation extremes affected

287 by multiple factors including the vertical velocity profile and temperature changes (O’Gorman and  
288 Schneider 2009).

289 The precipitation over WUS for moderate or heavy precipitation is mainly resulted from the  
290 large-scale water flux transport from the eastern Pacific Ocean rather than directly from evapora-  
291 tion, mainly in the form of atmospheric rivers (ARs) or orographic updraft (Trenberth et al. 2003;  
292 Neiman et al. 2008). The storm track may be enhanced, which would increase ARs along the U.S.  
293 west coast with increased air water vapor content in future [citation needed]. In the following sec-  
294 tion, both the mean changes of precipitation and precipitation distributions including non-extreme  
295 and extreme events will be investigated projected by the models under a extreme climate forcing  
296 context of RCP 8.5.

297 [Paul: Mention ENSO as a driver of precipitation here via modulation of the storm track. Discuss  
298 how there is uncertainty in our results as a consequence of uncertainty in the representation of  
299 ENSO. See if you can find a reference to the representation of ENSO in the coupled CESM.]

## 300 6. Results

### 301 a. Mean climatology

302 Before proceeding with the analysis of precipitation features, it is first important to understand  
303 how the mean climatology changes in VR-CESM across time periods (Figure 4). Since the charac-  
304 ter of WUS precipitation has a strong seasonal dependence, the mean climatology including mean  
305 precipitation, near-surface temperature and near-surface relative humidity are depicted in two sea-  
306 sons including the cool season (or wet season) from October to March and the warm season (or  
307 dry season) from April to September.

308 As a result of enhanced GHG concentrations, mean annual near-surface temperature (T2avg)  
309 increases by about 1.5 to 2 K from hist to mid and about 4 to 6 K from mid to end. Despite the  
310 large spatial variation in climatological temperatures, the temperature change between historical  
311 and future is fairly uniform. However, there is a slightly weaker increase in the near-coastal  
312 regions during cool season and in the lower latitude area at warm season, which might be due to  
313 the increased westerly wind during cool seasons and northward wind during warm season from  
314 the near ocean. Larger increases of temperature is also observed in warm season than cool season  
315 for about 0.5 K and 1 K for mid and end respectively.

316 Practically, whether the increase rate of the water vapor as the temperature goes up will keep the  
317 same or not will directly affect the relative humidity. As water vapor reaches saturation, condens-  
318 ation triggers clouds and precipitation. To understand the increasing rate of water vapor content  
319 under climate warming and whether relative humidity can be remain or not, 2m relative humidity  
320 (RH) is plotted in Figure 4.

321 Overall, RH remains almost the same as hist over the regions where temperature does not sub-  
322 stantially increase. However, in regions where temperature increase is larger than 2 K, RH is  
323 instead observed to decrease significantly relative to historical values for about 2% and 3-6%  
324 compared to mid and end respectively. In fact, trends in RH are spatially consistent with tempera-  
325 ture increase but opposite in magnitude with a spatial correlation coefficient of approximately 0.8.  
326 RH still remains the same or increase over part of the near-coastal area over the Pacific Ocean due  
327 to the lower increase of T2avg compared to the land area. This suggests that continental evapo-  
328 ration and oceanic water vapor transport are insufficient to compensate for the air vapor capacity  
329 when temperature increases to certain level, which is consistent with Joshi et al. (2008), and has  
330 been observed in results by Rowell and Jones (2006) over continental and southeastern Europe  
331 and Simmons et al. (2010) over low-latitude and midlatitude land areas.

332 Based on those background changes of heat and water vapor, from `hist` to `mid`, mean precipita-  
333 tion showed a 0.2-0.6 mm/day increase during cool season with a largest change over northwest  
334 and less than 0.2 mm/day during warm season over southeast part. From `hist` to `end`, the increase is  
335 about 0.4-1.2 mm/day during cool season with also a largest change over northwest, and no notable  
336 change is observed during warm season. Nonetheless, these results are statistically significant (see  
337 Figure 5). East of the Rockies, precipitation increases through mid-century (statistically signifi-  
338 cant), but this trend appears to recede towards the end of the century (although these results are not  
339 significant). There is also a decrease of about 0.1mm/day in total precipitation over the western  
340 flank of the Sierra Nevadas during the cool season from `hist` to future. This decrease (about 0.15  
341 mm/day) is also found over the Cascades and the western coastal area during warm season from  
342 `hist` to `mid`. However, this decrease is not statistically significant. Majority of the precipitation  
343 over the cool season emerged from large-scale patterns, whereas warm season precipitation was  
344 from convection processes.

345 The precipitation over WUS for moderate or heavy precipitation is mainly due to the large-  
346 scale water flux transport from the eastern Pacific Ocean rather than directly from evaporation,  
347 mainly in the form of atmospheric rivers or orographic updraft (Trenberth et al. 2003; Neiman  
348 et al. 2008). According to previous studies (e.g. (Allen and Ingram 2002; Allan and Soden 2008;  
349 O’Gorman and Schneider 2009; Min et al. 2011)), changes in more extreme precipitation follow  
350 the C-C relationship more closely than total precipitation precipitation amount (Trenberth et al.  
351 2003). In order to find out the precipitation changes in a comprehensive aspect based on our fine-  
352 scale simulations, analyses of different precipitation distributions are focused in the following part  
353 to account for the future changes of diverse precipitation events.

354 **Key questions that need to be answered here:**

- 355     ● Why does mean wet season precipitation increase over the northwest? Answer: Increased  
356         orographic precipitation due to increased IVT. IVT increases due to larger specific humidity  
357         from increased ocean evaporation, which is affected primarily by climatological forcing (?)
- 358     ● Why does precipitation stay the same over Southern California? Answer: No substantial  
359         predicted increase in IVT over E. Pac near Southern California coast. IVT in this region is  
360         driven primarily by variations in ENSO.
- 361     ● Why does precipitation stay the same over the Intermountain West? (Since precipitation over  
362         the Intermountain West during warm season is mainly results from the convection processes,  
363         the precipitation is directly related with the changes of the relative humidity. As shown in  
364         Figure 4, RH has decreased over most the study area except over where the soil moisture is  
365         relatively low. The changes of RH are related with the soil moisture magnitude accompanying  
366         the changes of latent heat flux during warm season.)

367     *b. Precipitation indices*

368     In order to find out the precipitation changes in a comprehensive aspect based on our fine-scale  
369         simulations, analyses of different precipitation distributions are focused in this part to account  
370         for the future changes of diverse precipitation events. [Paul: Previous sentence poorly written]  
371     The precipitation indices are presented in Table 1. For each index, the changes of precipitation  
372         character for each period, averaged over all ensemble members are plotted in Figure 5 (for the  
373         indices that quantify precipitation days) and Figure 6 (for the indices describing precipitation  
374         amounts). Although mean precipitation shows a weak but overall increasing trend from hist to  
375         mid and mid to end (about 10-15%), the precipitation indices exhibit substantially more unique  
376         character.

377 When comparing `hist` to `mid`, the total rainy days and frequency of non-extreme precipitation  
378 have significantly increased (about 10-15%) mainly over the central-east and southeast part of  
379 WUS, which is less obvious between `mid` and `end`. On the contrary, the frequency of non-extreme  
380 precipitation have decreased significantly over the northwest region and the eastern part of the  
381 Montana, Wyoming and Oregon from `mid` to `end` (about 10%). These changes are the primary  
382 driver for the observed change to mean precipitation exhibited in Figure 4.

383 As for extreme precipitation frequency (i.e. days with daily Pr between 10 mm and 40 mm), the  
384 number of days increases from `hist` to `mid`, but the pattern is scattered over northwest and central  
385 WUS. When comparing `mid` to `end`, there is a clear and significant increase in extreme precip-  
386 itation events over the northwest coastal area (about 20-30%) and eastern flank of the Cascades  
387 (larger than 40%). This result is consistent with Dominguez et al. (2012), who observe a robust  
388 increase in winter precipitation extremes toward the latter half of the 21st century by an ensemble  
389 of RCMs. There is a slight, but insignificant decrease over the Cascades and the Sierra Nevada  
390 (significance is low due to the high variability of precipitation). No notable predicted changes have  
391 been observed over California.

392 The associated precipitation signal under a warmer climate is more ambiguous for California  
393 (Neelin et al. 2013) considering the extreme variability on interannual time scales (Dettinger  
394 2011). Kim (2005) found that under global warming, heavy precipitation events show largest  
395 increases in the mountainous regions of the northern California Coastal Range and the Sierra  
396 Nevada. However, our results show a minor decrease (though not statistically significant) of ex-  
397 treme precipitation over the Sierra Nevada. The decrease over southwest U.S. is mainly due to the  
398 intensified La Niña in the future as shown in the Section 2.

399 For very extreme precipitation ( $\text{Pr} \geq 40 \text{ mm}$ ) events, there is an increasing trend over the north-  
400 west coast (larger than 60%) and the Cascades (about 50%) and its eastern flank (larger than 60%)

when comparing `hist` to `end`. Significant changes have also been observed over the northern mountainous part of California for about 20-40% from `hist` to `end`. The corresponding changes in rain amount are consistent with the changes of frequency (see Figure 6). Overall, these results indicate more extreme precipitation over the northwest U.S. with changes in precipitation extremes following more consistently with the C-C relationship.

In order to understand the drivers behind the observed changes, we first examine change in moisture flux for cool seasons when WUS precipitation is primarily from water vapor influx from the Pacific Ocean (see Figure 7). We observe an increase in specific humidity at 850 hPa that accompanies the increase of the temperature in future. However, when comparing to `hist`, wind patterns in `mid` and `end` are also reduced **over the eastern part of the WUS and enhanced to the west [where? I don't see it]**. Integrated vapor transport (IVT) (Figure 7) for extreme precipitation days over cool seasons. Generally, IVT is useful to understand extreme precipitation events that arise from atmospheric rivers over the northwestern U.S. and from orographic uplift (especially for very extreme precipitation) (Ralph et al. 2004; Leung and Qian 2009; Dettinger 2011). Based on the observed change in IVT, it is clear that the increase in moisture influx from past to future, which is mainly due to the change of the air water vapor content with increased temperature, corresponds to the changes of precipitation extremes shown in Figure 5.

## 1) QUANTILE CORRELATION ANALYSIS

To see if changes in mean precipitation can be used to predict changes in extreme precipitation features, the correlations between  $Pr$  and specific quantiles have been calculated. Here, selected quantiles including the values at 70% (70p), 80% (80p), 90% (90p), 95% (95p) and 99% (99p) are applied based on all the daily precipitation data at each grid point within each time period. These quantiles are chosen in order to account for the changes of both moderation and extreme

424 precipitation. The mean Pr and those quantiles for hist, and the differences of these quantities  
425 among different time periods can be found in the supplemental figure. Within expectation, regions  
426 with higher Pr are associated with larger values of those quantiles, i.e. stronger precipitation  
427 extremes. This is further supported by the high correlation (about 0.7-0.9) between Pr and R20mm,  
428 R40mm, and Rxmm, not between Pr and non-extreme precipitation events.

429 Spatial correlation is assessed by computing Pearson product-moment coefficient of linear corre-  
430 lation between relevant variables. It is found that the absolute changes of Pr in future are positively  
431 related with the absolute changes of the quantiles. This relationship is at a moderate level between  
432 mid and hist (larger than 0.65), and becomes stronger when going to the end period (reaching  
433 ~0.96). Consistently, the mean Pr itself is also positively correlated with the absolute changes of  
434 the quantiles in future (around 0.5 to 0.78), except 70p between end and mid and 99p mid and  
435 hist.

436 The relative changes of quantiles are also related with the relative changes of Pr with correla-  
437 tions around 0.65 to 0.85, except 70p and 80p between end and mid. So, the area featured with  
438 higher increase of extreme precipitations in future also tends to have larger increase of its mean  
439 precipitation. However, the wetter area does not necessary have more intense changes of moderate  
440 and extreme precipitation than drier area.

441 However, no notable consistent correlation is found between the changes of Pr and the changes  
442 of precipitation indices, further stating that mean precipitation and precipitation events undergo  
443 different features as for the changes in the future. [Paul: rewrite this sentence]

444 might divide into four regions; PDF of each region? [Paul: This is a good idea]

445 2) ISOLATING DIFFERENCES DUE TO CLIMATE CHANGE AND ENSO

446 The phase of ENSO is well known to have important repercussions on precipitation extremes  
447 (Larkin and Harrison 2005; Allan and Soden 2008; Maloney et al. 2014; Yoon et al. 2015). Cai  
448 et al. (2014) found a significantly increase for extraordinary precipitation along the eastern Pacific  
449 Ocean in the 21st century within the CMIP5 ensemble, associated with increasing frequency of  
450 extreme El Niño events due to greenhouse warming. In this part, we will figure out how the ENSO  
451 impacts specific regions over our study area, and whether the effects pattern will change over time.

452 (Huang: Yoon et al. (2015) found a strengthened relation with ENSO for the projected increase  
453 in water cycle extremes in California using the output from CESM1 and CMIP5. Similarly by  
454 Maloney et al. (2014) using CMIP5 dataset. (check the CESM1?))

455 ENSO from past to future, the difference of precipitation behaviors between the warm phase (i.e.  
456 El Niño) and cool phase (i.e. La Niña) of ENSO is illustrated in Figure 8 for the wet seasons of  
457 each time period. Based on the ONI index values, the mean SST anomalies are 1.38, 1.71 and 2.30  
458 K during El Niño years, and -1.16, -1.62 and -1.43 K during La Niña years for hist, mid and end  
459 respectively. The mean SSTs over the Niño 3.4 region where the are 26.83, 28.62 and 30.54°C  
460 for textsfhist, mid and end respectively. Based on the SST datasets we used here, the anomaly  
461 of ENSO has intensified. The SST anomalies of each year and each month, and their associated  
462 spatial pattern when averaged during the warm and cool phases can be found in the supplement,  
463 exhibiting the increasing frequency of El Niño during for mid and almost doubled frequency of La  
464 Niña during mid and end compared to the hist.

465 (Huang: As SSTs increase in the future, is not it normal for the anomaly of ENSO to be increased  
466 to compensate the changes of water vapor capacity? Might email Neale about this.)

467 During the El Niño phase, intensified mean precipitation is expected over the southwest (Ham-  
468 let and Lettenmaier 2007), along with reduced precipitation intensity over the northwest. In La  
469 Niña phase, the pattern is essentially reversed, with wetter conditions in the northwest and a drier  
470 situation in the Southwest. This feature is characterized as a northwest/southwest precipitation  
471 dipole, triggered by ENSO's modification of the storm track (Gershunov and Barnett 1998; Le-  
472 ung et al. 2003b), along with modulation of the enhanced precipitation variability (Cayan et al.  
473 1999; Kahya and Dracup 1994). This dipole is also apparently in the frequency of rainy days and  
474 extreme precipitation events.

475 In mid and hist, ENSO is observed to intensify, which appears to be related with the changes  
476 of the strength of El Niño and La Niña. This can be explained by the SST anomaly magnitude  
477 (detrended) of warm and cold phases (see the supplement). DeFlorio et al. (2013) also found a  
478 statistically significant linkages with ENSO and PDO for both the overall and extreme intensity  
479 of wintertime precipitation over the WUS using CCSM4 (earlier form of CESM). Strengthening  
480 storm patterns associated with ENSO are also found by Maloney et al. (2014) over California using  
481 CMIP5 output under RCP8.5.

482 We have also checked the teleconnection effect of Pacific Decadal Oscillation (PDO) and it  
483 did not show strong effect alone. Precipitation features did not change notably when at the cool  
484 phase or warm phase of PDO during hist. However, together with ENSO at the same phase,  
485 PDO can have notable effect over northwest. This coupled effect has been found by previous  
486 studies Gershunov and Barnett (1998), stating ENSO and PDO can "reinforce" each other with  
487 PDO responding to the same internal atmospheric variability as ENSO (Pierce 2002). In our  
488 simulations, the patterns of PDO index diverse [Paul: diverse?] a lot [Paul: "a lot" is too informal]  
489 from past to future, and we suppose that 26 years are not long enough to account for the variability  
490 of PDO due to its duration for decades. In this study, the PDO is not analyzed as its decadal

491 duration making it difficult to capture within the 26 years simulation time period. [Paul: I think  
492 you can say more than this – I recall you showing that there were roughly an equal number of  
493 positive PDO years and negative PDO years in the data]

494 The impact of ENSO is further observed by the IVT difference over rainy days between El Niño  
495 and La Niña (see Figure 9) accompanying by the wind pattern difference at 850 hPa, showing the  
496 increase of the moisture flux for the southwest and decrease for the northwest. This suggests the  
497 major role of moisture influx regulation of ENSO.

498 Based on the above results, it can be seen that the magnitude of the effects of ENSO is compara-  
499 ble or even higher than the impacts of climate forcing. For further investigation, linear regression  
500 is applied to signaling the factor effects due to ENSO and climate forcing. First, we get the SST  
501 anomaly of each cool season when ENSO mainly affect followed by the way of Niño 3.4 to be the  
502 ENSO factor values. Then, we use the GHGs values at each year to represent the climate forcing  
503 factor. The features of the precipitation indices as we defined above are used as response vari-  
504 ables. Combined the values of all the time period and all the runs, we got the significance of these  
505 two factors' effects at each grid point based on the ANOVA (analysis of variance) output (see the  
506 supplement). It seems that [informal] changing of the SSTs anomaly can affect most of the study  
507 area for non-extreme precipitation events, and southern regions and the Cascades and the Rocky  
508 Mountains for precipitation extremes. The GHGs factor mainly shows significant impacts over the  
509 northwest and inter-mountainous regions for both non-extreme and extreme precipitation events.

510 We have also examined the linear coefficients of these two factors over where their effects are  
511 significant to see the strength that ENSO and GHGs play at each grid point (see the supplement).  
512 It turns out that [informal – don't act too surprised] the effect of the ENSO is similar to the pattern  
513 of the difference between El Niño and La Niña (see Figure 9). In contrast, the effect of the GHGs  
514 is close to the pattern of the difference between the different time periods (see Figure 5). We do

515 acknowledge that the values might not be accurate due to the simple linear mode we used here.  
516 However, the qualitative conclusions won't change. Therefore, we assume that even the ENSO  
517 largely regulates the precipitation over different phases, it won't affect our results shown here for  
518 the changes of precipitation features from past to future. Although here is just one of the possible  
519 cases of ENSO scenarios in the future, as ENSO behavior is strongly dependent on choice of  
520 climate models, the underlying principles should still be consistent.

521 Although, the strength of ENSO intensifies in the future with CESM, there is still substantial  
522 uncertainty regarding how El Niño will change under global warming as debated by plenty of  
523 studies (Fedorov and Philander 2000; Guilyardi et al. 2009), particularly as ENSO appears to be  
524 relatively insensitive to a doubling of CO<sub>2</sub> in most models (DiNezio et al. 2012). Correctly simula-  
525 tion changes to the spatial pattern of SSTs ion state-of-the-art coupled GCMs remains challenging  
526 Joseph and Nigam (2006); Jha et al. (2014); Taschetto et al. (2014). Capotondi (2013) showed  
527 that the diversity of El Niño characteristics in CCSM4 is comparable to what was found in obser-  
528 vations, although, as found by Deser et al. (2012c), the overall magnitude of ENSO in CCSM4 is  
529 overestimated by 30% over the preindustrial time period.

## 530 7. Discussion and Summary

531 The increased cool season precipitation extremes tend to result in higher runoff events over  
532 the northwest U.S., which are in turn associated with a greater chance of flooding and a loss of  
533 snowpack. A decrease in counts of rainy days during the warm season over central and southern  
534 California, though small in magnitude, will probably intensify the drought condition due to the  
535 deficit of soil moisture with higher evapotranspiration caused by the warmer climate in the future  
536 Cayan et al. (2010); Bell et al. (2004).

537 (Summary is to be added once the main content have been settled down The contribution of  
538 human-induced increases in greenhouse gases to the character of precipitation is confounded by  
539 patterns of variability in the atmospheric circulation. Consistent with previous studies, changes  
540 in more extreme precipitation follow the Clausius-Clapeyron relationship more closely than total  
541 precipitation amount. The changes of the strength of ENSO remains uncertain. However, the char-  
542 acter of ENSO appears to be the largest factor in understanding changing precipitation extremes  
543 in the U.S. West.)

544 *Acknowledgments.* The authors would like to thank Michael Wehner for sharing the dataset and  
545 many suggestions. The authors also want to thank Alan M. Rhoades for providing the simulation  
546 output. We acknowledge the substantial efforts behind the datasets used in this study, including  
547 UW, NCDC and NARR. The simulation data used is available by request at xyhuang@ucdavis.edu.  
548 This project is supported in part by the xxx and by the xxx.

## 549 References

- 550 AchutaRao, K., and K. R. Sperber, 2006: Enso simulation in coupled ocean-atmosphere models:  
551 are the current models better? *Climate Dynamics*, **27** (1), 1–15.
- 552 Allan, R. P., and B. J. Soden, 2008: Atmospheric warming and the amplification of precipitation  
553 extremes. *Science*, **321** (5895), 1481–1484.
- 554 Allen, M. R., and W. J. Ingram, 2002: Constraints on future changes in climate and the hydrologic  
555 cycle. *Nature*, **419** (6903), 224–232.
- 556 Bell, J. L., L. C. Sloan, and M. A. Snyder, 2004: Regional changes in extreme climatic events: a  
557 future climate scenario. *Journal of Climate*, **17** (1), 81–87.

- 558 Cai, W., and Coauthors, 2014: Increasing frequency of extreme el niño events due to greenhouse  
559 warming. *Nature climate change*, **4** (2), 111–116.
- 560 Caldwell, P., 2010: California wintertime precipitation bias in regional and global climate models.  
561 *Journal of Applied Meteorology and Climatology*, **49** (10), 2147–2158.
- 562 Capotondi, A., 2013: Enso diversity in the ncar ccsm4 climate model. *Journal of Geophysical*  
563 *Research: Oceans*, **118** (10), 4755–4770.
- 564 Cayan, D. R., T. Das, D. W. Pierce, T. P. Barnett, M. Tyree, and A. Gershunov, 2010: Future  
565 dryness in the southwest us and the hydrology of the early 21st century drought. *Proceedings of*  
566 *the National Academy of Sciences*, **107** (50), 21 271–21 276.
- 567 Cayan, D. R., K. T. Redmond, and L. G. Riddle, 1999: ENSO and hydrologic extremes in the  
568 western United States\*. *Journal of Climate*, **12** (9), 2881–2893.
- 569 DeFlorio, M. J., D. W. Pierce, D. R. Cayan, and A. J. Miller, 2013: Western us extreme precipita-  
570 tion events and their relation to enso and pdo in ccsm4. *Journal of Climate*, **26** (12), 4231–4243.
- 571 Dennis, J., and Coauthors, 2011: CAM-SE: A scalable spectral element dynamical core for the  
572 Community Atmosphere Model. *International Journal of High Performance Computing Appli-*  
573 *cations*, 1094342011428142.
- 574 Deser, C., R. Knutti, S. Solomon, and A. S. Phillips, 2012a: Communication of the role of natural  
575 variability in future north american climate. *Nature Climate Change*, **2** (11), 775–779.
- 576 Deser, C., A. Phillips, V. Bourdette, and H. Teng, 2012b: Uncertainty in climate change projec-  
577 tions: the role of internal variability. *Climate Dynamics*, **38** (3-4), 527–546.
- 578 Deser, C., and Coauthors, 2012c: Enso and pacific decadal variability in the community climate  
579 system model version 4. *Journal of Climate*, **25** (8), 2622–2651.

- 580 Dettinger, M., 2011: Climate change, atmospheric rivers, and floods in California—a multimodel  
581 analysis of storm frequency and magnitude changes1. Wiley Online Library.
- 582 Diffenbaugh, N. S., J. S. Pal, R. J. Trapp, and F. Giorgi, 2005: Fine-scale processes regulate the  
583 response of extreme events to global climate change. *Proceedings of the National Academy of*  
584 *Sciences of the United States of America*, **102** (44), 15 774–15 778.
- 585 DiNezio, P. N., B. P. Kirtman, A. C. Clement, S.-K. Lee, G. A. Vecchi, and A. Wittenberg, 2012:  
586 Mean climate controls on the simulated response of ENSO to increasing greenhouse gases. *Journal*  
587 *of Climate*, **25** (21), 7399–7420.
- 588 Dominguez, F., E. Rivera, D. Lettenmaier, and C. Castro, 2012: Changes in winter precipitation  
589 extremes for the western United States under a warmer climate as simulated by regional climate  
590 models. *Geophysical Research Letters*, **39** (5).
- 591 Donat, M. G., A. L. Lowry, L. V. Alexander, P. A. OGorman, and N. Maher, 2016: More extreme  
592 precipitation in the world [rsquo] s dry and wet regions. *Nature Climate Change*.
- 593 Duffy, P., and Coauthors, 2006: Simulations of present and future climates in the western United  
594 States with four nested regional climate models. *Journal of Climate*, **19** (6), 873–895.
- 595 Duli re, V., Y. Zhang, and E. P. Salath  Jr, 2011: Extreme Precipitation and Temperature over the  
596 US Pacific Northwest: A Comparison between Observations, Reanalysis Data, and Regional  
597 Models\*. *Journal of Climate*, **24** (7), 1950–1964.
- 598 Easterling, D. R., G. A. Meehl, C. Parmesan, S. A. Changnon, T. R. Karl, and L. O. Mearns, 2000:  
599 Climate extremes: observations, modeling, and impacts. *science*, **289** (5487), 2068–2074.
- 600 Fedorov, A. V., and S. G. Philander, 2000: Is el ni o changing? *Science*, **288** (5473), 1997–2002.

- 601 Fox-Rabinovitz, M., J. Côté, B. Dugas, M. Déqué, and J. L. McGregor, 2006: Variable resolution  
602 general circulation models: Stretched-grid model intercomparison project (SGMIP). *Journal of*  
603 *Geophysical Research: Atmospheres (1984–2012)*, **111 (D16)**.
- 604 Fox-Rabinovitz, M. S., G. L. Stenchikov, M. J. Suarez, and L. L. Takacs, 1997: A finite-  
605 difference GCM dynamical core with a variable-resolution stretched grid. *Monthly weather*  
606 *review*, **125 (11)**, 2943–2968.
- 607 Frei, C., R. Schöll, S. Fukutome, J. Schmidli, and P. L. Vidale, 2006: Future change of precipita-  
608 tion extremes in Europe: Intercomparison of scenarios from regional climate models. *Journal*  
609 *of Geophysical Research: Atmospheres (1984–2012)*, **111 (D6)**.
- 610 Gao, Y., J. Lu, L. R. Leung, Q. Yang, S. Hagos, and Y. Qian, 2015: Dynamical and thermodynamical  
611 modulations on future changes of landfalling atmospheric rivers over western north america.  
612 *Geophysical Research Letters*, **42 (17)**, 7179–7186.
- 613 Gates, W. L., 1992: AMIP: The Atmospheric Model Intercomparison Project. *Bulletin of the*  
614 *American Meteorological Society*, **73**, 1962–1970.
- 615 Gershunov, A., and T. P. Barnett, 1998: Interdecadal modulation of enso teleconnections. *Bulletin*  
616 *of the American Meteorological Society*, **79 (12)**, 2715–2725.
- 617 Grodsky, S. A., J. A. Carton, S. Nigam, and Y. M. Okumura, 2012: Tropical atlantic biases in  
618 ccsm4. *Journal of Climate*, **25 (11)**, 3684–3701.
- 619 Guilyardi, E., A. Wittenberg, A. Fedorov, M. Collins, C. Wang, A. Capotondi, G. J. Van Olden-  
620 borg, and T. Stockdale, 2009: Understanding el niño in ocean-atmosphere general circulation  
621 models. *Bulletin of the American Meteorological Society*, **90 (3)**, 325.

- 622 Hamlet, A. F., and D. P. Lettenmaier, 2005: Production of Temporally Consistent Gridded Precipi-  
623 tation and Temperature Fields for the Continental United States\*. *Journal of Hydrometeorology*,  
624 **6** (3), 330–336.
- 625 Hamlet, A. F., and D. P. Lettenmaier, 2007: Effects of 20th century warming and climate variability  
626 on flood risk in the western us. *Water Resources Research*, **43** (6).
- 627 Hegerl, G. C., F. W. Zwiers, P. A. Stott, and V. V. Kharin, 2004: Detectability of anthropogenic  
628 changes in annual temperature and precipitation extremes. *Journal of Climate*, **17** (19), 3683–  
629 3700.
- 630 Huang, X., A. M. Rhoades, P. A. Ullrich, and C. M. Zarzycki, 2016: An evaluation of the vari-  
631 able resolution-cesm for modeling california’s climate. *Journal of Advances in Modeling Earth*  
632 *Systems*.
- 633 Huang, X., and P. A. Ullrich, 2016: Irrigation impacts on california’s climate with the variable-  
634 resolution cesm. *Journal of Advances in Modeling Earth Systems*.
- 635 Hurrell, J. W., J. J. Hack, D. Shea, J. M. Caron, and J. Rosinski, 2008: A new sea surface temper-  
636 ature and sea ice boundary dataset for the Community Atmosphere Model. *Journal of Climate*,  
637 **21** (19), 5145–5153.
- 638 Hurrell, J. W., and Coauthors, 2013: The community earth system model: A framework for col-  
639 laborative research. *Bulletin of the American Meteorological Society*, **94** (9), 1339–1360.
- 640 Jha, B., Z.-Z. Hu, and A. Kumar, 2014: Sst and enso variability and change simulated in historical  
641 experiments of cmip5 models. *Climate dynamics*, **42** (7-8), 2113–2124.
- 642 Joseph, R., and S. Nigam, 2006: Enso evolution and teleconnections in ipcc’s twentieth-century  
643 climate simulations: Realistic representation? *Journal of Climate*, **19** (17), 4360–4377.

- 644 Joshi, M. M., J. M. Gregory, M. J. Webb, D. M. Sexton, and T. C. Johns, 2008: Mechanisms for  
645 the land/sea warming contrast exhibited by simulations of climate change. *Climate Dynamics*,  
646 **30** (5), 455–465.
- 647 Kahya, E., and J. A. Dracup, 1994: The influences of type 1 el nino and la nina events on stream-  
648 flows in the pacific southwest of the united states. *Journal of Climate*, **7** (6), 965–976.
- 649 Kao, H.-Y., and J.-Y. Yu, 2009: Contrasting eastern-pacific and central-pacific types of enso.  
650 *Journal of Climate*, **22** (3), 615–632.
- 651 Karl, T. R., N. Nicholls, and A. Ghazi, 1999: Clivar/gcos/wmo workshop on indices and indicators  
652 for climate extremes workshop summary. *Weather and Climate Extremes*, Springer, 3–7.
- 653 Kharin, V. V., F. W. Zwiers, X. Zhang, and G. C. Hegerl, 2007: Changes in temperature and  
654 precipitation extremes in the IPCC ensemble of global coupled model simulations. *Journal of  
655 Climate*, **20** (8), 1419–1444.
- 656 Kim, J., 2005: A projection of the effects of the climate change induced by increased co2 on  
657 extreme hydrologic events in the western us. *Climatic Change*, **68** (1-2), 153–168.
- 658 Laprise, R., and Coauthors, 2008: Challenging some tenets of regional climate modelling. *Meteo-  
659 rology and Atmospheric Physics*, **100** (1-4), 3–22.
- 660 Larkin, N. K., and D. Harrison, 2005: On the definition of el niño and associated seasonal average  
661 us weather anomalies. *Geophysical Research Letters*, **32** (13).
- 662 Leung, L. R., L. O. Mearns, F. Giorgi, and R. L. Wilby, 2003a: Regional climate research: needs  
663 and opportunities. *Bulletin of the American Meteorological Society*, **84** (1), 89–95.

- 664 Leung, L. R., and Y. Qian, 2009: Atmospheric rivers induced heavy precipitation and flooding in  
665 the western US simulated by the WRF regional climate model. *Geophysical research letters*,  
666 **36** (3).
- 667 Leung, L. R., Y. Qian, and X. Bian, 2003b: Hydroclimate of the western United States based on  
668 observations and regional climate simulation of 1981-2000. Part I: Seasonal statistics. *Journal*  
669 *of Climate*, **16** (12), 1892–1911.
- 670 Maloney, E. D., and Coauthors, 2014: North american climate in cmip5 experiments: part iii:  
671 assessment of twenty-first-century projections\*. *Journal of Climate*, **27** (6), 2230–2270.
- 672 Maurer, E., A. Wood, J. Adam, D. Lettenmaier, and B. Nijssen, 2002: A long-term hydrologically  
673 based dataset of land surface fluxes and states for the conterminous United States\*. *Journal of*  
674 *climate*, **15** (22), 3237–3251.
- 675 McDonald, A., 2003: Transparent boundary conditions for the shallow-water equations: testing in  
676 a nested environment. *Monthly weather review*, **131** (4), 698–705.
- 677 Meehl, G. A., H. Teng, and G. Bannister, 2006: Future changes of el niño in two global coupled  
678 climate models. *Climate Dynamics*, **26** (6), 549–566.
- 679 Mesinger, F., and K. Veljovic, 2013: Limited area NWP and regional climate modeling: a test  
680 of the relaxation vs Eta lateral boundary conditions. *Meteorology and Atmospheric Physics*,  
681 **119** (1-2), 1–16.
- 682 Mesinger, F., and Coauthors, 2006: North American regional reanalysis. *Bulletin of the American*  
683 *Meteorological Society*, **87**, 343–360.
- 684 Min, S.-K., X. Zhang, F. W. Zwiers, and G. C. Hegerl, 2011: Human contribution to more-intense  
685 precipitation extremes. *Nature*, **470** (7334), 378–381.

- 686 Neale, R. B., and Coauthors, 2010a: Description of the NCAR community atmosphere model  
687 (CAM 5.0). *NCAR Tech. Note NCAR/TN-486+STR*.
- 688 Neale, R. B., and Coauthors, 2010b: Description of the NCAR Community Atmosphere Model  
689 (CAM 5.0). NCAR Technical Note NCAR/TN-486+STR, National Center for Atmospheric Re-  
690 search, Boulder, Colorado, 268 pp.
- 691 Neelin, J. D., B. Langenbrunner, J. E. Meyerson, A. Hall, and N. Berg, 2013: California winter  
692 precipitation change under global warming in the coupled model intercomparison project phase  
693 5 ensemble. *Journal of Climate*, **26** (17), 6238–6256.
- 694 Neiman, P. J., F. M. Ralph, G. A. Wick, J. D. Lundquist, and M. D. Dettinger, 2008: Meteorolog-  
695 ical characteristics and overland precipitation impacts of atmospheric rivers affecting the west  
696 coast of north america based on eight years of ssm/i satellite observations. *Journal of Hydrom-  
697 eteorology*, **9** (1), 22–47.
- 698 NOAA, 2013: Defining El Niño and La Niña. Accessed: 2015-  
699 08-20, [https://www.climate.gov/news-features/understanding-climate/  
700 watching-el-nio-and-la-nia-noaa-adapts-global-warming](https://www.climate.gov/news-features/understanding-climate/watching-el-nio-and-la-nia-noaa-adapts-global-warming).
- 701 O’Gorman, P. A., and T. Schneider, 2009: The physical basis for increases in precipitation ex-  
702 tremes in simulations of 21st-century climate change. *Proceedings of the National Academy of  
703 Sciences*, **106** (35), 14 773–14 777.
- 704 Oleson, K., and Coauthors, 2010: Technical description of version 4.0 of the Community Land  
705 Model (CLM). NCAR Technical Note NCAR/TN-478+STR, National Center for Atmospheric  
706 Research, Boulder, Colorado, 257 pp. doi:10.5065/D6FB50WZ.

- 707 Pierce, D. W., 2002: The role of sea surface temperatures in interactions between enso and the  
708 north pacific oscillation. *Journal of climate*, **15** (11), 1295–1308.
- 709 Ralph, F. M., P. J. Neiman, and G. A. Wick, 2004: Satellite and caljet aircraft observations of  
710 atmospheric rivers over the eastern north pacific ocean during the winter of 1997/98. *Monthly*  
711 *Weather Review*, **132** (7), 1721–1745.
- 712 Rauscher, S. A., E. Coppola, C. Piani, and F. Giorgi, 2010: Resolution effects on regional climate  
713 model simulations of seasonal precipitation over Europe. *Climate dynamics*, **35** (4), 685–711.
- 714 Rauscher, S. A., T. D. Ringler, W. C. Skamarock, and A. A. Mirin, 2013: Exploring a Global  
715 Multiresolution Modeling Approach Using Aquaplanet Simulations. *Journal of Climate*, **26** (8),  
716 2432–2452.
- 717 Rhoades, A. M., X. Huang, P. A. Ullrich, and C. M. Zarzycki, 2015: Characterizing Sierra Nevada  
718 snowpack using variable-resolution CESM. *Journal of Applied Meteorology and Climatology*,  
719 **(2015)**.
- 720 Riahi, K., and Coauthors, 2011: RCP 8.5A scenario of comparatively high greenhouse gas emis-  
721 sions. *Climatic Change*, **109** (1-2), 33–57.
- 722 Rowell, D. P., and R. G. Jones, 2006: Causes and uncertainty of future summer drying over europe.  
723 *Climate Dynamics*, **27** (2-3), 281–299.
- 724 Salathé Jr, E. P., R. Steed, C. F. Mass, and P. H. Zahn, 2008: A High-Resolution Climate Model  
725 for the US Pacific Northwest: Mesoscale Feedbacks and Local Responses to Climate Change\*.  
726 *Journal of Climate*, **21** (21), 5708–5726.
- 727 Scoccimarro, E., M. Zampieri, A. Bellucci, A. Navarra, and Coauthors, 2013: Heavy precipitation  
728 events in a warmer climate: results from CMIP5 models. *Journal of climate*.

- 729 Seneviratne, S. I., and Coauthors, 2012: Changes in climate extremes and their impacts on the  
730 natural physical environment. *Managing the risks of extreme events and disasters to advance*  
731 *climate change adaptation*, 109–230.
- 732 Sillmann, J., V. Kharin, F. Zwiers, X. Zhang, and D. Bronaugh, 2013: Climate extremes indices  
733 in the cmip5 multimodel ensemble: Part 2. future climate projections. *Journal of Geophysical*  
734 *Research: Atmospheres*, **118 (6)**, 2473–2493.
- 735 Simmons, A., K. Willett, P. Jones, P. Thorne, and D. Dee, 2010: Low-frequency variations  
736 in surface atmospheric humidity, temperature, and precipitation: Inferences from reanalyses  
737 and monthly gridded observational data sets. *Journal of Geophysical Research: Atmospheres*,  
738 **115 (D1)**.
- 739 Singh, D., M. Tsiang, B. Rajaratnam, and N. S. Diffenbaugh, 2013: Precipitation extremes over the  
740 continental United States in a transient, high-resolution, ensemble climate model experiment.  
741 *Journal of Geophysical Research: Atmospheres*, **118 (13)**, 7063–7086.
- 742 Small, R. J., and Coauthors, 2014: A new synoptic scale resolving global climate simulation using  
743 the community earth system model. *Journal of Advances in Modeling Earth Systems*, **6 (4)**,  
744 1065–1094.
- 745 Staniforth, A. N., and H. L. Mitchell, 1978: A variable-resolution finite-element technique for  
746 regional forecasting with the primitive equations. *Monthly Weather Review*, **106 (4)**, 439–447.
- 747 Sugi, M., and J. Yoshimura, 2004: A mechanism of tropical precipitation change due to co2  
748 increase. *Journal of climate*, **17 (1)**, 238–243.

- 749 Taschetto, A. S., A. S. Gupta, N. C. Jourdain, A. Santoso, C. C. Ummenhofer, and M. H. England,  
750 2014: Cold tongue and warm pool enso events in cmip5: mean state and future projections.  
751 *Journal of Climate*, **27 (8)**, 2861–2885.
- 752 Taylor, M. A., 2011: Conservation of mass and energy for the moist atmospheric primitive equa-  
753 tions on unstructured grids. *Numerical Techniques for Global Atmospheric Models*, Springer,  
754 357–380.
- 755 Tebaldi, C., K. Hayhoe, J. M. Arblaster, and G. A. Meehl, 2006: Going to the extremes. *Climatic  
756 change*, **79 (3-4)**, 185–211.
- 757 Trenberth, K. E., 2011: Changes in precipitation with climate change. *Climate Research*, **47 (1)**,  
758 123.
- 759 Trenberth, K. E., A. Dai, R. M. Rasmussen, and D. B. Parsons, 2003: The changing character of  
760 precipitation. *Bulletin of the American Meteorological Society*, **84 (9)**, 1205–1217.
- 761 Walker, M. D., and N. S. Diffenbaugh, 2009: Evaluation of high-resolution simulations of daily-  
762 scale temperature and precipitation over the united states. *Climate dynamics*, **33 (7-8)**, 1131–  
763 1147.
- 764 Wehner, M. F., 2013: Very extreme seasonal precipitation in the NARCCAP ensemble: model  
765 performance and projections. *Climate Dynamics*, **40 (1-2)**, 59–80.
- 766 Wehner, M. F., R. L. Smith, G. Bala, and P. Duffy, 2010: The effect of horizontal resolution  
767 on simulation of very extreme US precipitation events in a global atmosphere model. *Climate  
768 dynamics*, **34 (2-3)**, 241–247.

- 769 Wehner, M. F., and Coauthors, 2014: The effect of horizontal resolution on simulation qual-  
770 ity in the Community Atmospheric Model, CAM5.1. *J. Model. Earth. Sys.*, doi:10.1002/  
771 2013MS000276.
- 772 Yoon, J.-H., S. S. Wang, R. R. Gillies, B. Kravitz, L. Hipps, and P. J. Rasch, 2015: Increasing  
773 water cycle extremes in California and in relation to ENSO cycle under global warming. *Nature*  
774 *communications*, **6**.
- 775 Zarzycki, C. M., C. Jablonowski, and M. A. Taylor, 2014: Using Variable-Resolution Meshes  
776 to Model Tropical Cyclones in the Community Atmosphere Model. *Monthly Weather Review*,  
777 **142** (3), 1221–1239.
- 778 Zarzycki, C. M., C. Jablonowski, D. R. Thatcher, and M. A. Taylor, 2015: Effects of localized grid  
779 refinement on the general circulation and climatology in the Community Atmosphere Model.  
780 *Journal of Climate*, **(2015)**.
- 781 Zhang, X., L. Alexander, G. C. Hegerl, P. Jones, A. K. Tank, T. C. Peterson, B. Trewin, and  
782 F. W. Zwiers, 2011: Indices for monitoring changes in extremes based on daily temperature and  
783 precipitation data. *Wiley Interdisciplinary Reviews: Climate Change*, **2** (6), 851–870.
- 784 Zhang, X., J. Wang, F. W. Zwiers, and P. Y. Groisman, 2010: The influence of large-scale climate  
785 variability on winter maximum daily precipitation over North America. *Journal of Climate*,  
786 **23** (11), 2902–2915.
- 787 update the mesh grid plot
- 788 update the plot with new label levels

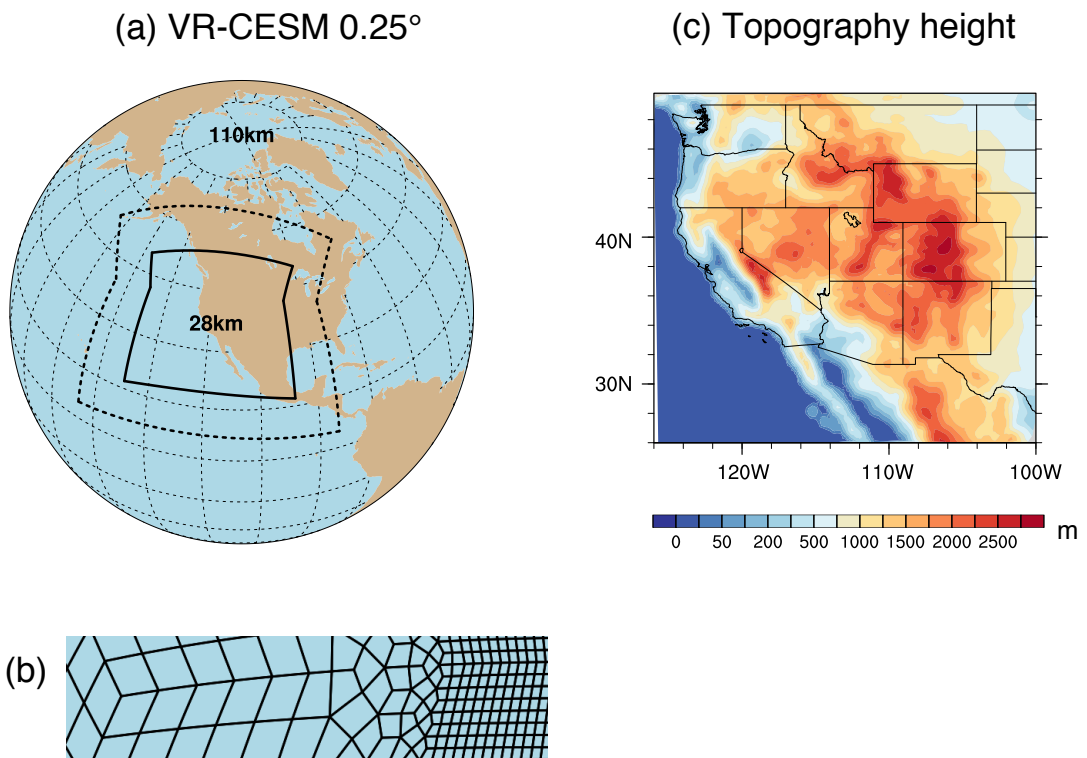
789 LIST OF TABLES

TABLE 1. Precipitation indices employed in this study.

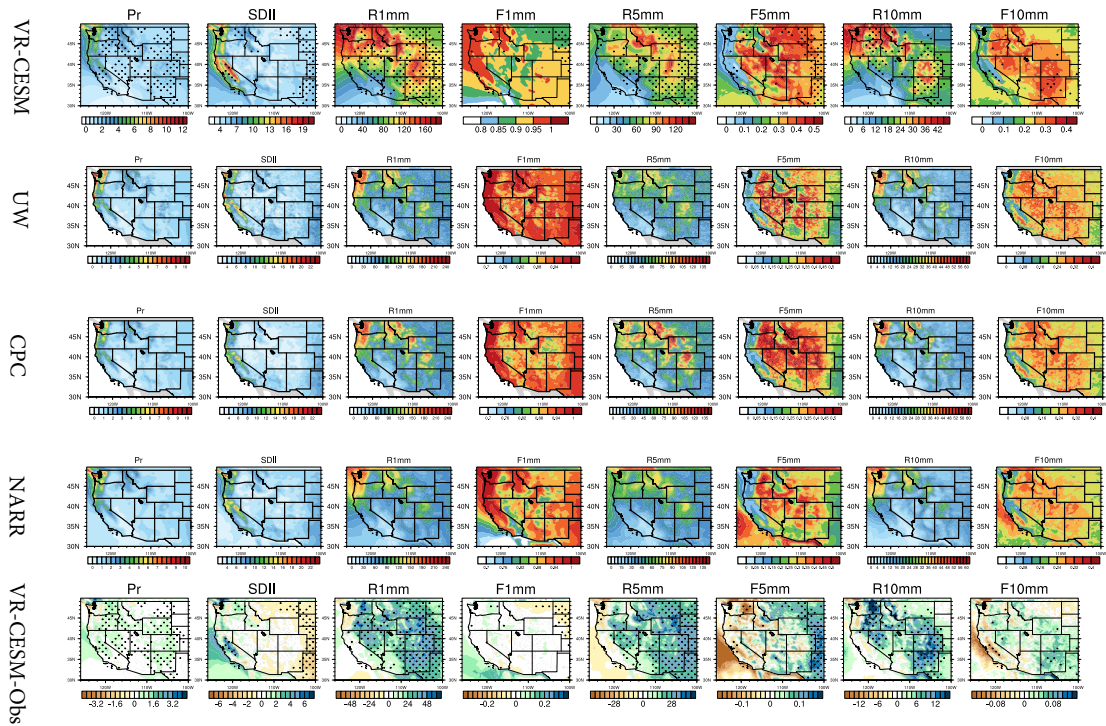
Name	Definition
Pr	Mean daily precipitation
R1mm	Number of days per year with Pr>1 mm
SDII	Simple precipitation intensity index: Precipitation amount / $\langle R1mm \rangle$ (mm/day)
R5mm	Number of days per year with Pr>1 mm and Pr=<5 mm
R10mm	Number of days per year with Pr>5 mm and Pr=<10 mm
R20mm	Number of days per year with Pr>10 mm and Pr=<20 mm
R40mm	Number of days per year with Pr>20 mm and Pr=<40 mm
Rxmm	Number of days per year with Pr>40 mm
F1mm	Fraction of precipitation contributed to the total precipitation for days of R1mm (similarly for F5mm, F10mm, F20mm, F40mm and Fxmm)
P5mm	Precipitation amount from R5mm (similarly for P10mm, P20mm, F40mm, Pxmm)

791 **LIST OF FIGURES**

792 <b>Fig. 1.</b>	(a) The approximate grid spacing used for the VR-CESM $0.25^\circ$ mesh. (b) A depiction of 793 the transition from the global $1^\circ$ resolution mesh through two layers of refinement to $0.25^\circ$ . 794 (c) Topography height over the study area. . . . .	41
795 <b>Fig. 2.</b>	Mean precipitation and other related indices from VR-CESM and reference datasets over 796 1980-2005. (Note: Grids with statistically significance difference are marked with stip- 797 pling.) . . . . .	42
798 <b>Fig. 3.</b>	The mean precipitation and other related indices from VR-CESM and reference datasets 799 over 1980-2005 (continued). . . . .	43
800 <b>Fig. 4.</b>	The mean precipitation ( $Pr$ ), 2m average temperature ( $T2avg$ ), and 2m relative humidity 801 ( $RH$ ) averaged over each time period. (Note: Grids with statistically significance difference 802 for the $RH$ are marked with stippling.) . . . . .	44
803 <b>Fig. 5.</b>	Differences of precipitation behaviors from past to future over WUS averaged of each time 804 period. (Note: Grids with statistically significance difference are marked with stippling.) . . . . .	45
805 <b>Fig. 6.</b>	Differences of precipitation behaviors from past to future over WUS averaged of each time 806 period (continued). . . . .	46
807 <b>Fig. 7.</b>	Changes of specific humidity and horizontal wind pattern at 850hPa for moisture flux il- 808 lustration, and IVT for simulations under different time period of wet season (October to 809 March). (Note: The minimum wind vector is set to be 0.5 m/s, therefore, the wind less than 810 0.5 m/s is also plotted at the minimum length for better visualization.) <b>For all difference</b> 811 <b>plots, make sure to use a common [min,max] range as its currently difficult to tease out dif-</b> 812 <b>ferences. Difference plots should also use a different color table to the mean results (perhaps</b> 813 <b>a single color color table?).</b> . . . . .	47
814 <b>Fig. 8.</b>	Difference of precipitation behaviors between warm and cool phases of ENSO from past to 815 future over WUS averaged of each time period. . . . .	48
816 <b>Fig. 9.</b>	Changes of IVT for simulations under different phases of ENSO of wet season (October to 817 March). (Note: The minimum wind vector is set to be 0.5 m/s, therefore, the wind less than 818 0.5 m/s is also plotted at the minimum length for better visualization.) . . . . .	49

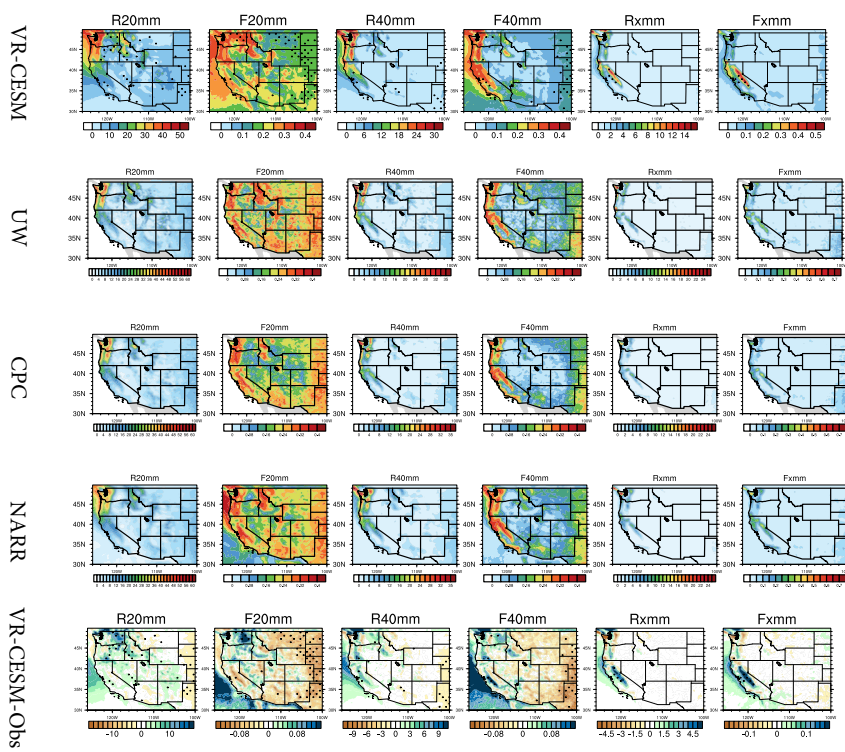


819 FIG. 1. (a) The approximate grid spacing used for the VR-CESM  $0.25^\circ$  mesh. (b) A depiction of the transition  
 820 from the global  $1^\circ$  resolution mesh through two layers of refinement to  $0.25^\circ$ . (c) Topography height over the  
 821 study area.

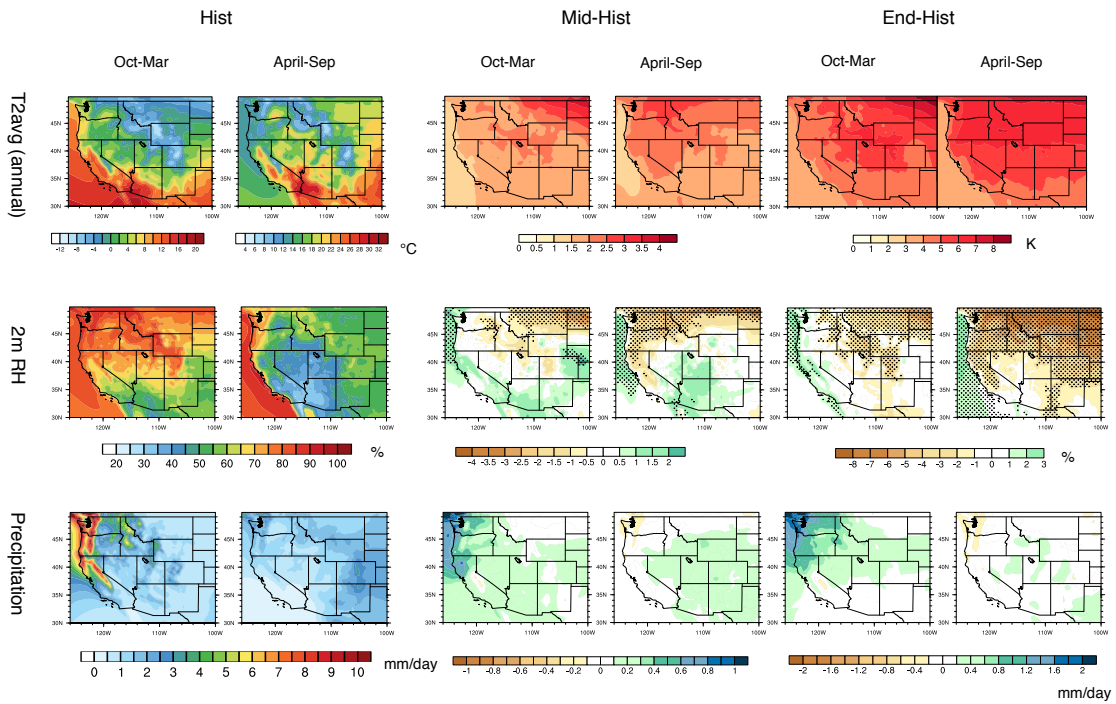


822 FIG. 2. Mean precipitation and other related indices from VR-CESM and reference datasets over 1980-2005.

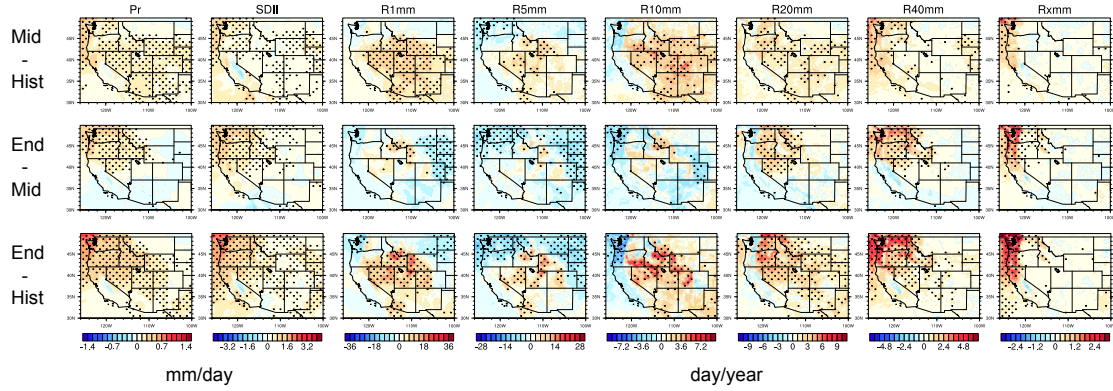
823 (Note: Grids with statistically significant difference are marked with stippling.)



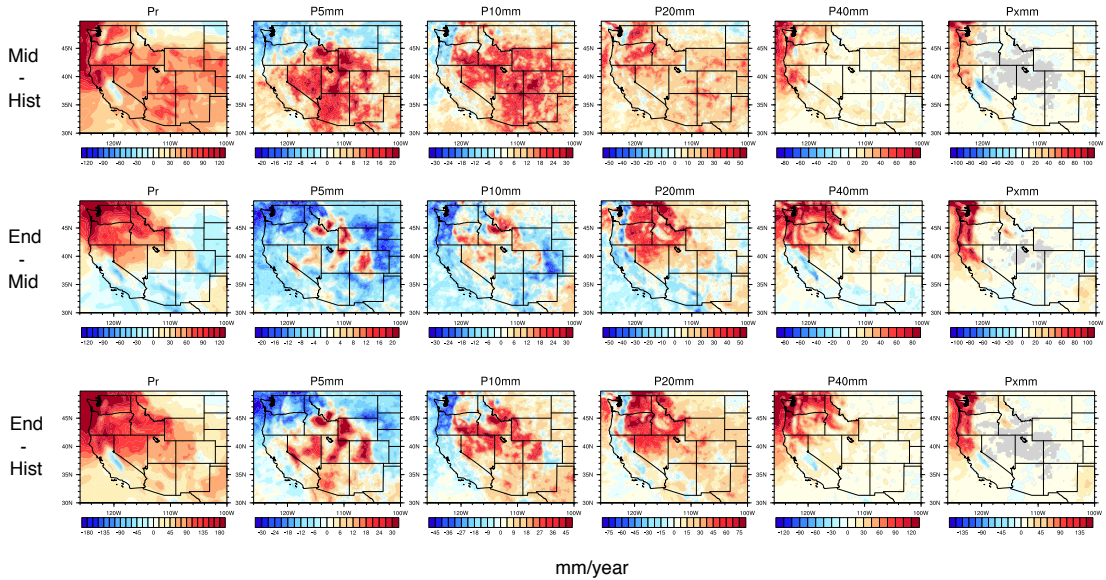
824 FIG. 3. The mean precipitation and other related indices from VR-CESM and reference datasets over 1980-  
 825 2005 (continued).



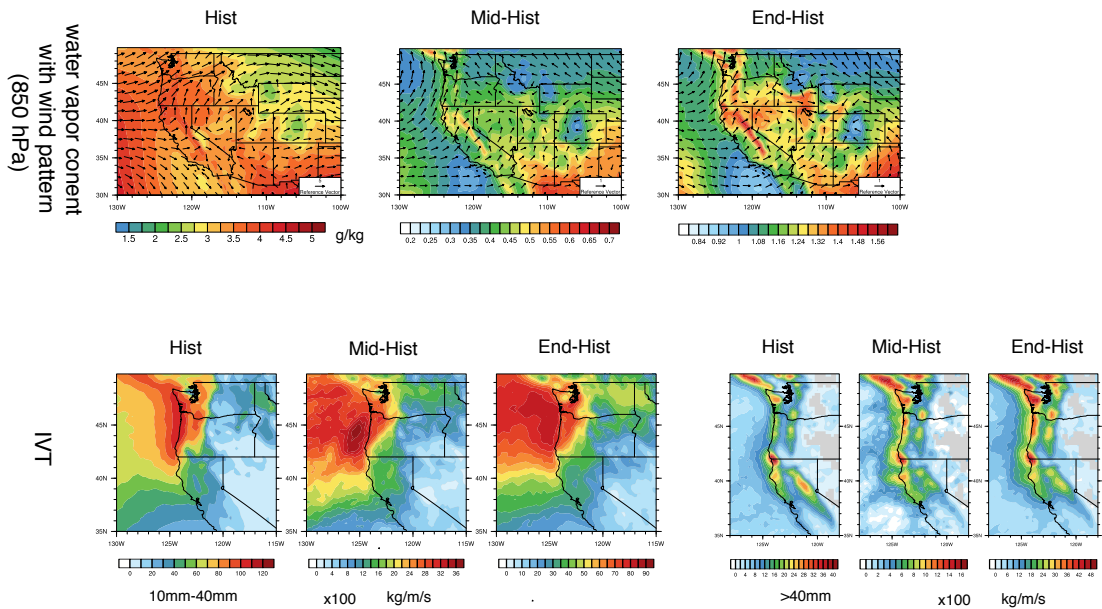
826 FIG. 4. The mean precipitation (Pr), 2m average temperature (T2avg), and 2m relative humidity (RH) aver-  
 827 aged over each time period. (Note: Grids with statistically significant difference for the RH are marked with  
 828 stippling.)



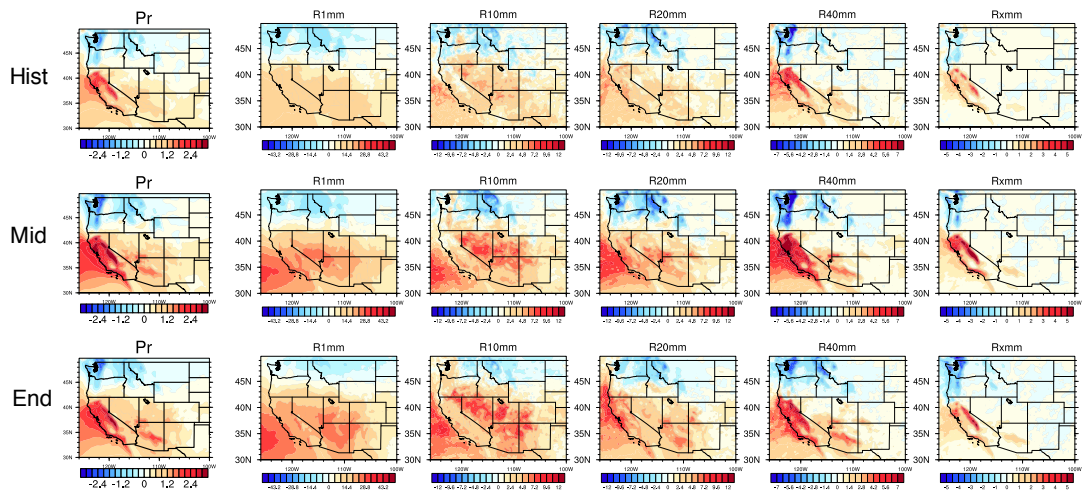
829 FIG. 5. Differences of precipitation behaviors from past to future over WUS averaged of each time period.  
 830 (Note: Grids with statistically significance difference are marked with stippling.)



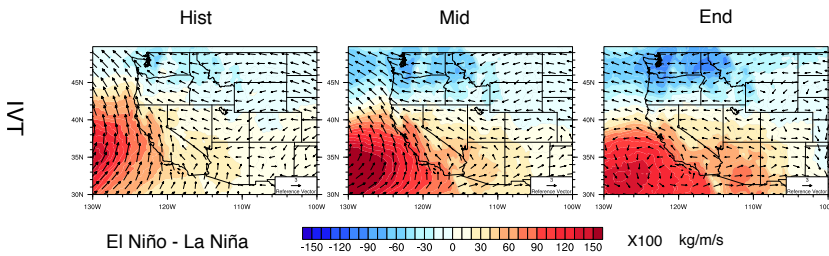
831 FIG. 6. Differences of precipitation behaviors from past to future over WUS averaged of each time period  
 832 (continued).



833 FIG. 7. Changes of specific humidity and horizontal wind pattern at 850hPa for moisture flux illustration, and  
 834 IVT for simulations under different time period of wet season (October to March). (Note: The minimum wind  
 835 vector is set to be 0.5 m/s, therefore, the wind less than 0.5 m/s is also plotted at the minimum length for better  
 836 visualization.) For all difference plots, make sure to use a common [min,max] range as its currently difficult  
 837 to tease out differences. Difference plots should also use a different color table to the mean results (perhaps a  
 838 single color color table?).



839 FIG. 8. Difference of precipitation behaviors between warm and cool phases of ENSO from past to future  
 840 over WUS averaged of each time period.



841 FIG. 9. Changes of IVT for simulations under different phases of ENSO of wet season (October to March).  
 842 (Note: The minimum wind vector is set to be 0.5 m/s, therefore, the wind less than 0.5 m/s is also plotted at the  
 843 minimum length for better visualization.)